



Design and architecture of a slender and flexible underwater robot

Jia-Lin Wang¹ · Jia-Ling Song^{1,2} · Ai-Rong Liu¹ · Jia-Qiao Liang¹ · Fo-Bao Zhou¹ · Jia-Jian Liang¹ · Ji-Yang Fu¹ · Bing-Cong Chen¹

Received: 11 May 2023 / Accepted: 27 March 2024 / Published online: 6 May 2024
© The Author(s) 2024

Abstract

This paper presents the design and analysis of a biomimetic underwater snake-like robot, addressing the main limitations of current underwater robotic systems in terms of maneuverability and adaptability in complex environments. The innovative design incorporates flexible joint modules that significantly enhance the robot's ability to navigate through narrow and irregular terrains, which is a notable limitation in traditional rigidly connected underwater robots. These flexible joints provide increased degrees of freedom and enable the robot to absorb and release energy, ensuring stability even under external impacts, thus extending the operational lifespan of the robot. Finite element analysis demonstrates the flexible joints' superior performance in various underwater conditions, offering a greater range of motion and workspace compared to rigid connections. The results indicate that the robot's modular design, combined with the flexible joint module, leads to improved agility and maneuverability, allowing for precise and intentional operation. The control module, equipped with advanced sensors and a CPU, manages the complex dynamics introduced by the flexible joints, ensuring effective navigation and operation. The specific advantages of this design include the robot's enhanced structural integrity, its ability to conform to irregular surfaces, and its adaptability to environmental variations. The paper concludes with a discussion on the implications of these findings for the future design and operation of underwater serpentine robots, emphasizing the need for a balance between the effects of elastic modulus and workspace to maximize the benefits of flexible joints.

Keywords Underwater robot · Snake-like robot · Robot design · Flexible joint · Propulsion system

1 Introduction

Since the advent of underwater vehicles, there has been a transformative progression in the exploration of marine resources. This encompasses marine biodiversity, energy reserves, archaeological treasures, and geological formations. These vehicles not only unlock the mysteries of the deep but also serve as invaluable tools during environmental or man-made disasters, providing access to hazardous regions. Additionally, they play a pivotal role in infrastructure assessments and construction inspections [1]. With the burgeoning growth of marine industries and offshore engineering, the typology of underwater vehicles has diversified. Among these, the snake-like robot stands out. Its

unique design enables it to navigate confined spaces, such as pipelines, offshore energy infrastructures, underwater foundational piles, coral mazes, and intricate terrains. This is attributed to its compact cross-sectional profile, exceptional flexibility, and motion stability.

Biomimetic robots, a cornerstone of bionic technology, are witnessing a surge in engineering applications. These robots emulate various aquatic entities, ranging from fish, octopuses, and jellyfish to starfish, turtles, and scallops [2–4]. A recent innovation in this realm is a beaver-inspired hind limb underwater robot, crafted specifically for intricate underwater navigation [5]. Snakes, with their elongated, limbless form and adaptability across diverse terrains, have become a focal point for the development of snake-like robots.

In 1972, Shigeo Hirose introduced the pioneering snake-like robot, ACM-III [6, 7]. Comprising 20 sequentially connected rigid modules, this avant-garde creation mirrored the vertebrate structure and kinematic principles inherent to snakes. Each module was powered by an individual motor system, facilitating fluid, snake-like movement. Successive

✉ Ai-Rong Liu
liuar@gzhu.edu.cn

¹ Research Center for Wind Engineering and Engineering Vibration, Guangzhou University, Guangzhou, China

² Poly Chang Da Engineering Co., Ltd., Guangzhou, China

iterations of the ACM robots showcased enhanced designs and advanced control mechanisms suitable for diverse terrains. For instance, ACM-R3 and ACM-R4 utilized orthogonal bending joints for versatile navigation [7, 8]. The ACM-R5 was a landmark innovation, demonstrating proficiency in both terrestrial and aquatic environments, even executing underwater tumbling maneuvers [7]. The design ethos of the ACM series was anchored in multi-link articulated wheeled joints.

Another innovative series, the AIRO, was pioneered by Hirose's research team. These robots, specifically designed for pipeline inspections, utilized spherical wheels to seamlessly navigate and circumnavigate within pipes [9]. A standout model, the AIRO-2.2, introduced a shadow-based operational assistant technique. This method facilitated the identification of pipeline shapes and ensured autonomous navigation through both linear and meandering pipes [10]. Cornell Wright and his team conceptualized a unique snake-like robot. This design featured fully rigid modules interconnected by orthogonal joints. Such a configuration allowed for a comprehensive 180° rotation, with each module capable of rotating up to 90° relative to its preceding module. This design innovation ensured versatile locomotion, rotation, and 3-D climbing capabilities [11]. The SEA Snake series introduced another design nuance. These robots employed rubber-based torsional springs, ensuring elastic actuation between adjacent modules. This feature not only enhanced flexibility but also augmented controller capabilities for holistic body movements. As a result, these robots showcased adaptability across diverse terrains, including grasslands, tree trunks, and pipes [10, 11]. Further advancements in snake-like robotics were seen in the "Perambulator" and "Explorer" series. These amphibious robots, products of the Shenyang Institute of Automation from the Chinese Academy of Sciences, epitomized the adaptability and versatility of snake-inspired designs [12, 13].

In the evolving landscape of robotic design, multi-module snake-like robots predominantly feature rigid joints and are equipped with wheels [1, 9–11, 14]. These design choices have proven effective for facilitating diverse movements on terrestrial terrains. Early iterations of snake-like robots utilized passive wheels for vertical support at environmental contact points. Their efficiency was augmented with the inclusion of additional wheels or supports. For instance, Hirose's ACM III showcased 20 wheeled modules, while ACM-R3 and Crespi's AmphiBot I and II had wheels centrally positioned on each joint [4–6, 15–17]. However, the utility of passive wheels was confined to relatively even terrains. To navigate more challenging environments, active propulsion mechanisms, such as motorized wheels or pedrail tracks, were integrated. Hirose's ACM-R4, for instance, featured a mechanism driving wheels at each joint [7]. Liljebäck

et al.'s Mamba employed rubber wheels powered by singular servo motors [18]. Klaassen et al.'s GMD-Snake 2, designed to emulate the rectilinear movement of snakes, utilized belly scales to enhance traction and propulsion [19]. Other robots, like Borenstein's OmniTread Series [20, 21] and Siegwart's Proboscis robot [22], incorporated bellows-like linkages, ensuring adaptability in challenging terrains.

The integration of watertight and protective features in snake-like robots enables their operation in a variety of environments, especially underwater. For instance, Kelasidi, Liljebäck, and their colleagues pioneered the development of an amphibious snake-like robot named "Mamba." This robot is adept at performing both lateral undulation and eel-like movements [18, 23]. While snake-like robots designed for land can exhibit diverse movements such as sine wave, side winding, and rolling, mimicking these movements underwater is more challenging due to the heightened energy requirements and diminished efficacy. Traditional underwater vehicles predominantly utilize propellers and rudders for movement. However, the advent of elastic joints and multi-propulsion actuators signals a transformative shift in the compliance control of underwater snake-like robots. For example, while AmphiBot I and II are equipped with wheels for land-based movement, they also incorporate caudal fins to generate thrust underwater [16, 17, 24].

Propellers remain the primary propulsion mechanism for underwater vehicles, chosen for their efficiency and ease of control. A notable advancement in this domain is the Eelume, a second-generation snake-like robot crafted by Liljebäck's team in 2017. This multi-propeller underwater robot [25] features two distinct propulsion modules: one for longitudinal thrust with propellers on either side of its body, and another for lateral movement with internal horizontal and vertical propellers. The subsequent iteration, EELY500, enhanced motility by optimizing propeller placement and also boasted improved battery longevity and increased storage capacity [26]. Choset and his team introduced a unique design approach with a slender snake-like robot that utilized axial propulsion at its rear, concealing all propellers within its structure [27]. In a similar vein of innovation, Tang et al. [28] integrated the gliding attributes of underwater gliders into their snake-like robot. This three-dimensional design, equipped with five pitch-yaw joints and telescopic joints, demonstrated exceptional gliding mobility and pitch control, as confirmed by pool tests.

Underwater snake-like robots are celebrated for their adaptability. However, they face a primary challenge: ensuring efficient locomotion. This challenge is rooted in the underactuated motion control system, a limitation brought about by the robot's sophisticated flexible mechanics. In the domain of underwater soft robots, integrating servo motors and gear pumps is standard practice. These elements drive movement by altering the robot's form, a process achieved by

anchoring with tendon wires followed by tension application [3]. Interestingly, this design methodology is infrequently used for snake-like robots that have sturdier exteriors.

Nevertheless, merging elastic joints with multi-propulsion actuators emerges as a promising strategy to boost compliance control in underwater snake-like robots. This paper introduces a groundbreaking underwater snake-like robot, notable for its exceptional flexibility and agility, specifically designed for inspecting underwater structures in tight spaces. The design showcases the latest innovations in elastic joints and multi-propulsion actuation. A key highlight is the elastic joint mechanism, which incorporates springs in parallel, displaying a stiffness gradient from the center outward. Additionally, the integration of a multi-propeller control system offers an avant-garde solution to the robot's actuation and control dilemmas.

In the ensuing sections, this paper delves into pertinent works related to underwater robot designs, drawing particular attention to comparisons with established designs. The biomimetic structure, taking cues from snake physiology, and its integration into the robot's design are meticulously expounded upon. The robot's modular design is comprehensively delineated, highlighting the inclusion of diverse sensors, omnidirectional propulsion modules, and flexible joint modules. Further, the architecture and capabilities of the control module are detailed, accompanied by an in-depth discussion on strategies for optimizing motion control. The paper also presents the outcomes of finite element simulation experiments, juxtaposing them with results from other systems. In conclusion, the paper encapsulates the primary insights and innovations introduced, while also suggesting avenues for future exploration.

2 Biomimetic structure

2.1 Biomimetic locomotion and mechanism

Snakes possess a highly sophisticated musculoskeletal system and locomotion. Their skeleton primarily consists of a vast number of vertebrae, typically ranging from 200 to 400. While the relative rotation between individual vertebrae is small (horizontal rotation of 10° – 20° and vertical rotation of 2° – 3°), when accumulated across the entire body, these rotations enable the snake's characteristic movement. This movement is achieved through continuous muscle contractions and relaxations, leading to periodic changes in body shape that propel the snake forward.

Snakes exhibit various locomotion modes to adapt to different environments, such as lateral undulation, sidewinding, rectilinear movement, and concertina motion. Lateral undulation, in particular, is the most common terrestrial locomotion mode for snakes and the only mode for aquatic

locomotion [29]. However, the mechanism of lateral undulation differs between terrestrial and aquatic environments. On land, snakes move by leveraging anisotropic friction at contact points between their skin and the ground. In contrast, underwater, snakes generate movement by pushing against the water, similar to the swimming motion of eels. The large amplitude body bend undulations in eels, which allow at least one full wavelength to be transferred along their entire body while swimming, result in minimal yaw moment and a tendency for recoil, providing low swimming speed and excellent maneuverability [30]. Studies have indicated that the motion pattern of eels can be generalized as a sinusoidal traveling wave from head to tail with a constant amplitude [13, 15, 31, 32]. This motion can be described for the underwater lateral undulation of snakes using the following two-dimensional follow equation:

$$y(x, t) = A(x) \sin \left[2\pi \left(\frac{x}{\lambda} + \frac{t}{T} \right) \right] \quad (1)$$

where t represents time; x signifies the body's midline; y denotes the lateral displacement; and $A(x)$, λ , and T represent the amplitude, length, and period of the traveling waves, respectively.

Snake-inspired robots often emulate the snake's musculoskeletal system. However, they tend to overlook the intricate morphology of snake muscles. Typically, these robots consist of multiple rigid modules connected sequentially by joints. They achieve movement by replicating the sinusoidal motion of real snakes, primarily using servo motors within each module. In essence, while these robots mimic snake movement, they do not fully capture the nuanced driving patterns inherent to snake muscles.

2.2 Rotational joints

The snake's musculoskeletal system is intricate, characterized by its relatively straightforward vertebrae. Each vertebra comprises an anterior section, termed the vertebral body, and a posterior segment, known as the vertebral arch. The vertebral arch of one vertebra fuses with the centrum of its neighboring vertebra, forming an arthrosis reminiscent of a ball hinge. The snake's rotational movement arises from variations in muscle strength and elongation, presenting significant challenges for replication in mechanical joints with today's technology.

Consequently, snake-inspired robots have adopted alternative mechanical joint designs, including parallel, orthogonal, and universal joints. Parallel joints, essentially pairs of parallel chain bars, connect modules in series perpendicular to the robot's longitudinal axis, facilitating lateral bending. Hirose's ACMIII is a notable example of robots employing parallel joints [6, 7].

Orthogonal joints, on the other hand, enable three orthogonal translational rotations by altering the orientation of adjacent joints. These joints, while maintaining a singular motor and parallel linkage, support 3-D movements with a straightforward control mechanism. For instance, ACM-R3, equipped with orthogonal joints, can perform a range of movements, such as pedal wave, lateral rolling, and sinus-lifting [7, 8].

Universal joints, spherical in design, allow for any relative rotation between neighboring modules, granting robots a wide range of 3-D motions. Robots with these joints, like Hirose's amphibious ACM-R5, exhibit enhanced mobility and adaptability to various environments. This robot, in particular, features a sealed design with flexible bellows and an aluminum exterior [5]. Similarly, other robots like GMD-Snake2 by Linnemann et al., SSR-II by Takeshi et al. and the Orochi series by Takanash et al. from NEC [33–35], have also extensively incorporated universal joints.

3 Robot design

3.1 Design objectives and features

This paper introduces a novel snake-like underwater robot tailored for operations in challenging environments. The robot's design emphasizes the following key characteristics:

- **Compactness** crafted for narrow spaces, the robot's slender body allows it to navigate areas inaccessible to conventional underwater robots like ROVs and AUVs. Its elongated form ensures ample space for internal components.
- **Lightweight & Buoyancy** the robot's design prioritizes weight efficiency, facilitating longer distance travel with reduced energy. Its buoyancy is meticulously calibrated to be near neutral, minimizing energy used for vertical movement.
- **Waterproofing & Pressure Resistance** the robot's exterior, made from materials like aluminum alloy and rubber, is both waterproof and pressure-resistant. This ensures consistent weight and buoyancy by averting water ingress.
- **Modularity** adhering to modular design principles, the robot's components are function-based. This includes propulsion, power, actuation, rotational joints, and sensors. Such modularity enhances adaptability, as modules can be individually controlled, added, removed, or repaired.
- **Agility** the robot boasts high flexibility and maneuverability, capable of lateral undulation—a primary forward motion technique. Its design also supports various movements, from docking in flowing water and 3-D rolling to U-turns, vital for navigating intricate environments like pipes, offshore platform infrastructures, and coral reefs.

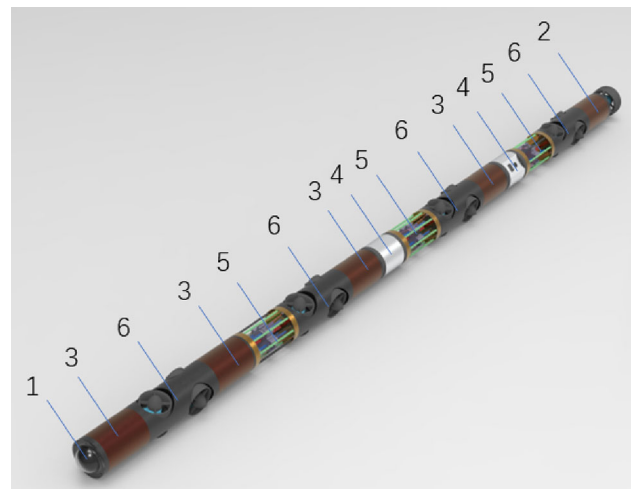


Fig. 1 The underwater snake-like robot: 1 head module, 2 tail module, 3 control module, 4 rotating head module, 5 flexible joint module, 6 omnidirectional thruster module

The robot boasts a modular construction, meticulously tailored for the inspection of underwater structures in challenging environments, such as within pipes or amidst intricate terrains. Its streamlined design, free from any protrusions, eliminates the risk of entanglement with aquatic vegetation. As illustrated in Fig. 1, the robot consists of a head module (labelled as 1), a tail module (labelled as 2), numerous cavity modules, and a variety of movable modules. These include a rotating head (labelled as 4), a flexible joint module (labelled as 5), and an omnidirectional thruster module (labelled as 6). Additionally, several control modules (labelled as 3) play a crucial role in the robot's functionality.

The design presented in this document enables the robot to operate autonomously, eliminating the need for power supply from large vessels, as it utilizes a 22.2 V battery for direct power to the body. This design offers improved flexibility compared to the Eelume snake-like robot and is suitable for smaller diameter pipes. While both designs employ motors to adjust the cable and control its curvature to navigate various pipe turns, the proposed design enables adjustments in pitch and yaw angles within a range of $\pm 90^\circ$. In contrast, the Eelume snake-like robot offers adjustments within a narrower range of $\pm 60^\circ$ (Table 1).

3.2 Sensing and observation systems

The underwater snake-like robot, designed for inspecting challenging underwater structures and intelligently analyzing their health status, is equipped with a comprehensive sensing system and specialized observation tools.

Table 1 Relevant parameters between this design and Eelume [25, 26]

Parameters	System	
	Eelume [25, 26]	This design
Depth rating	150 m	120 m
Diameter	Ø180 mm	Ø114 mm
Vehicle weight	75 kg	24 kg
Operating voltage	300 V	22.2V
Degree of freedom (yaw, pitch)	2 (± 60°)	2 (± 90°)

3.2.1 Head and cavity modules

The head module of the robot features a transparent protective cover and an LED bubble. This LED bubble acts as supplementary lighting, proving essential in both shallow and deep waters. The semispherical design of the cover minimizes hydraulic resistance, while the LED bubble sheds light in the deep water’s darkness, aiding in the observation of aquatic creatures that might scatter in the presence of intense light.

The cavity module, encapsulated within a cylindrical outer shell sealed by hot melt adhesives, houses a range of sensors. These include a temperature sensor, a pressure sensor, a Doppler velocimeter, and a six-axis accelerometer. The spacious design of the cavity module ensures that these sensors are well-arranged and protected.

3.2.2 Sensing and data processing system

The flexible snake-like underwater robot introduced in this research is specifically designed to inspect underwater structures in challenging environments and intelligently analyze their health status to detect potential structural issues. This robot incorporates two distinct sensing systems: an environmental perception sensor system for gathering hydrological data to guide its movement, and an ultrasonic sensor system dedicated to structural damages inspection. All these sensors are interconnected with the control module, facilitating seamless electronic data exchange.

As depicted in Fig. 2, the sensors housed within the cavity modules, which include the temperature sensor, pressure sensor, Doppler flowmeter, and a six-axis accelerometer, are responsible for collecting data on the water flow surrounding the robot. This data is then relayed to the microcomputer within the control module for processing. Once processed, the results are transmitted to the ground terminal and displayed on its screen.

Additionally, the rotating head of the robot is equipped with sensors that gather inspection data. The exposed camera captures optical imagery, while the ultrasonic probe records

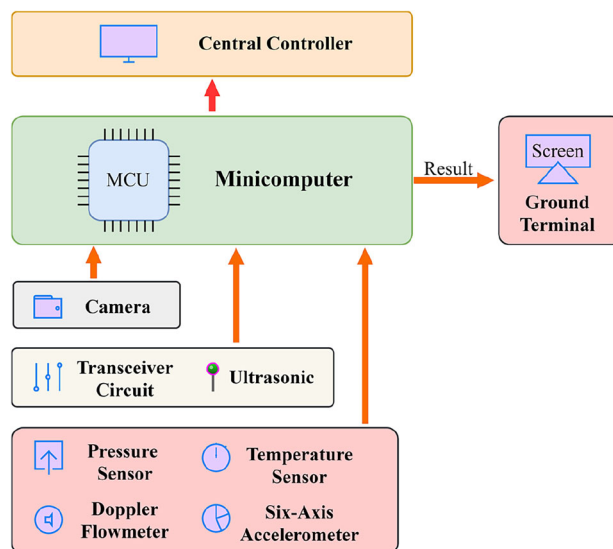


Fig. 2 The sensor system

acoustic images. The visual images are directly related to the ground terminal by the microcomputer for in-depth structural damage analysis. It is worth noting that the transceiver circuit acts as a supplementary component for the ultrasonic probe. During its operation, the transceiver circuit emits ultrasonic waves directed at the target structure. The signals reflected from the surface of the detected objects, along with the emitted ultrasonic waves, are captured by the ultrasonic probe. These retrieved signals are then sent to the microcomputer via the transceiver circuit, where they undergo filtering and Fourier transformation to produce a visual image for analysis.

3.3 Rotating head module

Delving into the specifics, in Fig. 1, the head module is securely attached to either the omnidirectional thruster module or the rotating head via a cavity module. This connection is fortified using sealed gaskets and fasteners. The fastener exerts a pre-retraction force and is complemented by a rubber ring at the connection point. In a similar fashion, the tail module is connected to another omnidirectional thruster module or rotating head via a cavity module. Furthermore, the forward thruster is strategically mounted on the tail module using a bracket.

The rotating head module, as depicted in Fig. 3, is a complex assembly comprising a protective sleeve, pedestal, bearing, an exposed camera, and an ultrasonic probe (labeled 41 to 45). Some internal components, such as the steering engine, remain concealed and are thus not labelled. The protective sleeve plays a crucial role in shielding the camera and ultrasonic probe. The pedestal, on the other hand, accommodates the steering engine. A waterproof bearing seamlessly

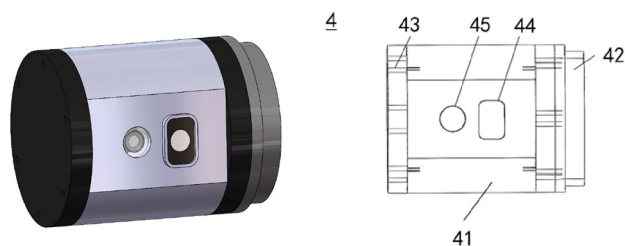


Fig. 3 The rotating head module

connects the protective sleeve and the pedestal, with a waterproof gasket positioned at their interface to prevent any water leakage. This gasket is further connected to the flexible joint module at the pedestal's end. It's noteworthy that all electronic components housed within the rotating head module are interconnected with the central control module.

3.4 Omnidirectional propulsion system

The underwater robot's propulsion system is an intricate amalgamation of several omnidirectional thruster modules paired with a primary forward thruster situated in the tail module. Each omnidirectional module, designed with multi-screw mechanics, features a set of vertically symmetrical propellers for yaw control and another set of horizontally symmetrical propellers for pitch control. These are commonly identified as the yaw and pitch thrusters. These modules can produce both lateral and vertical propulsion either independently or in tandem.

Mirroring the natural articulation of a snake's vertebrae, the flexible joint modules ensure fluid inter-module movement. In a coordinated assembly of movable modules, the omnidirectional thruster modules dictate the motion of their corresponding flexible joint modules, resulting in harmonious and fluid movements throughout the robot.

Further enhancing its capabilities, the rotating head module is equipped with an exposed camera and an ultrasonic probe, dedicated to capturing visual data. The tail module, anchoring the robot's end, houses both the forward thruster, which generates axial propulsive force, and a bracket that provides structural support, firmly connecting to the module ahead.

In this design, the P75 thruster (HYDROCEAN, China) is selected as the power source for the snake-like robot. The P75 is one of the most extensively used thrusters in the underwater robotics field, capable of delivering a maximum forward thrust of 5 kg and a maximum reverse thrust of 4 kg. The PWM signals sent from the controller to the P75 thruster require conversion through an electronic speed controller (ESC) to function properly. The process of thruster control is depicted in Fig. 4.

The transmission frequency of the PWM signals must be maintained at 50 Hz (20 ms). The thruster halts operation when the duty cycle is at 1500 μ s. It operates in reverse when the duty cycle ranges between 1100 and 1475 μ s, and it moves forward when the duty cycle is between 1525 and 1900 μ s. The dead zone, where the thruster remains inactive, spans from 1475 to 1525 μ s.

As illustrated in Fig. 5, the comprehensive omnidirectional thruster module is composed of an outer shell, brushless motors, thrusters, sealing rings, and fasteners, labeled sequentially from 61 to 65. The yaw thruster and pitch thruster are orthogonally and securely mounted within the outer shell, aligned parallel to the robot's axis, and are hermetically sealed from each other. The shafts of the propellers extend out from the outer shell, with two brushless motors situated in the middle of each twin propeller set to connect with them. These brushless motors can control the twin propellers to produce varying rotational movements in response to pulse width modulation signals received from the driver board, which in turn gets its control signal from the central processor. Given the symmetrical arrangement of the twin propellers, the dynamic characteristics of the thruster remain consistent. This design facilitates sensitive and swift orientation adjustments through the counter-rotation of the twin propellers, leading to a more substantial thrust output.

3.5 Flexible joint mechanism

The snake-like robot features an innovative flexible joint design, consisting of two interconnected endplates, a traction controller, three distinct spring sets, and multiple hauling cables. Figure 6a demonstrates how the two endplates are directly connected by these springs. The design's effectiveness hinges on the strategic arrangement and stiffness of the springs: The innermost spring (depicted in red) is the stiffest with a 1000 N/m rating, the intermediate spring (depicted in blue) is the most flexible with a 200 N/m stiffness, and the outermost spring (depicted in green) has a 500 N/m stiffness. This setup enables a variety of deformation capabilities, allowing the robot to fluidly adjust its movement posture by changing the angle between consecutive modules. The varying spring stiffnesses contribute to smoother joint deformations, bolstering the robot's structural integrity, mitigating deformation impacts, and prolonging its service life.

Figure 6a provides a detailed view of the flexible joint, while Fig. 6b zooms in on the hauling cables (labeled 57). These steel wire cables are divided into two groups by the traction controller, with each group's end securely attached to the inner side of an endplate, and the other end connected to the traction controller. The joint module also includes fixed bobbins (labeled 59) to guide the hauling cables. Additionally, the interconnected endplates are made from a weldable alloy metal.

Fig. 4 Architecture diagram of thruster control

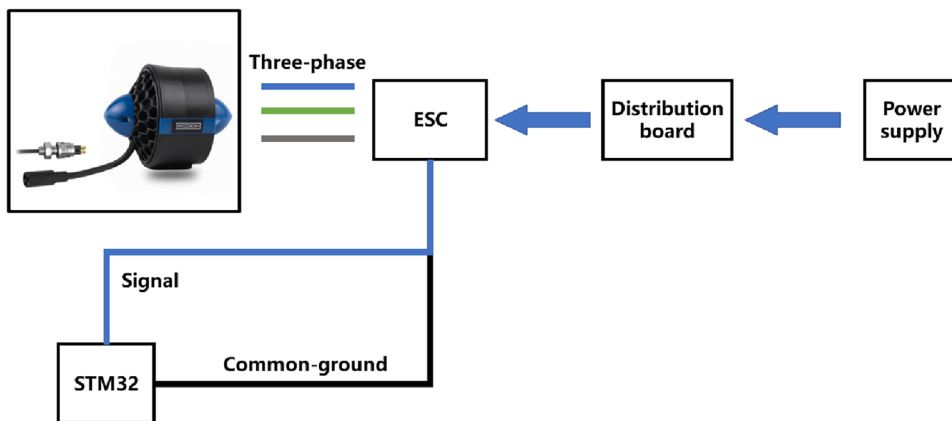
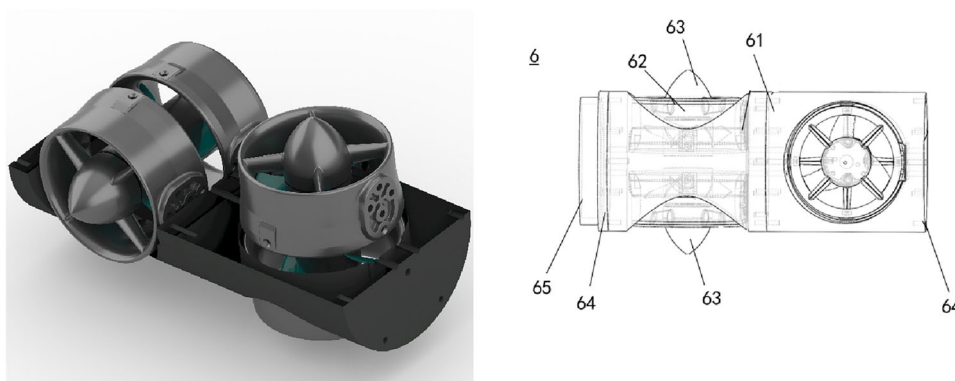


Fig. 5 Omnidirectional thruster module



The traction controller, depicted in Fig. 6c, is crucial for the joint’s functionality. Positioned between the endplates, it manipulates their movement through the hauling cables. This controller comprises a main frame, a steering engine, several reels, and both driving and follower gears, labeled sequentially from 581 to 585 in Fig. 6c and d. Controlled by the steering engine, the reels wind the hauling cables, causing the driving gear to propel the follower gear, which in turn rotates the reel shaft. As the reels rotate, the hauling cables extend linearly, prompting the interconnected endplates to move. The main frame features multiple apertures to accommodate the three spring sets, ensuring that when the hauling cables adjust the endplates’ position, the springs effectively distribute the deformation force across adjacent modules.

Incorporating the state-of-the-art flexible joints and omnidirectional thruster modules, this underwater snake-like robot stands distinct from its contemporaries. Its propulsion system, characterized by hyper-redundancy, empowers the robot with a diverse range of motion attitudes. The design of the flexible joint, with its layered rigidity structure, facilitates a spectrum of motion adjustments and transitions between various locomotion modes. This structure, featuring springs arranged from the innermost to the outermost with decreasing stiffness, ensures optimal flexibility.

Furthermore, the flexible joint module is adept at energy absorption and release, ensuring stability even under external

impacts. This not only augments the robot’s resilience against external forces but also extends its operational lifespan. The mechanical design of these joints has also streamlined the control over the robot’s bending deformations. When paired with the omnidirectional thruster modules, the robot exemplifies a harmonious blend of precision and agility in its underwater operations.

3.6 Control module

The control module acts as the “brain” of the underwater robot, expertly orchestrating its movements, collecting data, and interacting with the environment. It includes essential components like a dedicated battery, a driver with a transceiver circuit and microcomputer, a central processing unit (CPU) for managing sensor data, storage, and command distribution, and an Ultrasonic Communication Unit for communication, especially during autonomous patrol. The CPU analyzes sensor data to issue accurate commands to the propulsion system and steering engines, ensuring precise and intentional operation.

The snake-like robot’s hardware control system consists of an onshore ground station (PC), an upper computer, and a lower computer on the robot. The lower computer sends depth and attitude signals to the upper computer, which forwards them to the ground station. After processing these signals

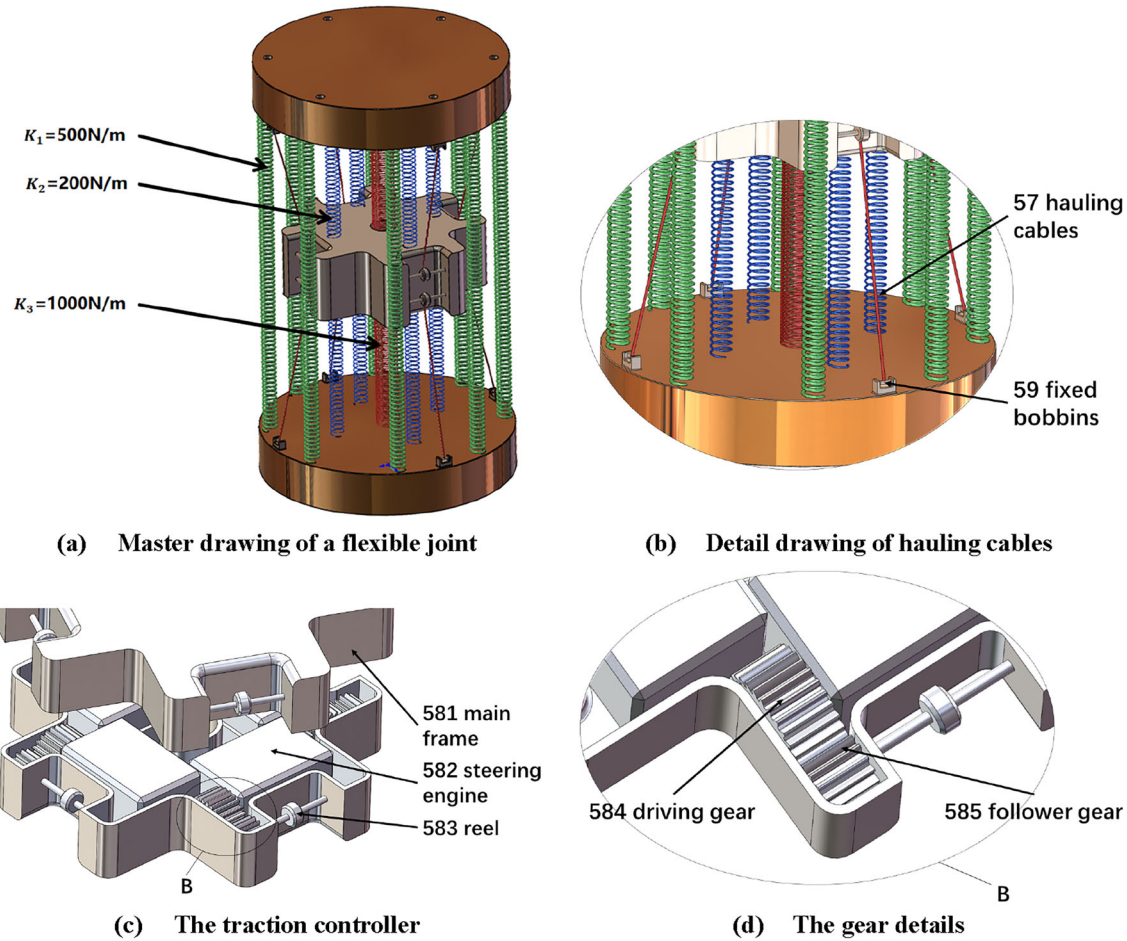


Fig. 6 The draft of flexible joint (color figure online)

using a control algorithm, the ground station sends PWM signals back to the upper computer, which then transmits them to the lower computer. This establishes a closed-loop control system, enabling precise underwater motion control as depicted in Fig. 7.

3.6.1 Hardware components

Upper computer The Raspberry Pi 4B (Raspberry Pi Foundation, U.K.), with 8 GB of RAM and a 32 GB memory card running Ubuntu 18.04 and ROS-melodic, is pivotal in the snake-like robot, serving as its central processing unit. It handles raw sensor data, communicates with the onshore computer, and outputs PWM signals for controllers. Connected to an IMX377 camera for image processing and an M750D sonar for underwater environment observation, it plays a vital role in the robot’s functionality.

Adopting a “PC + Embedded” architecture, the Raspberry Pi acts as the robot’s control system, while the PC facilitates remote monitoring. As shown in Fig. 8, the Raspberry Pi manages data acquisition and chassis control, and the PC can

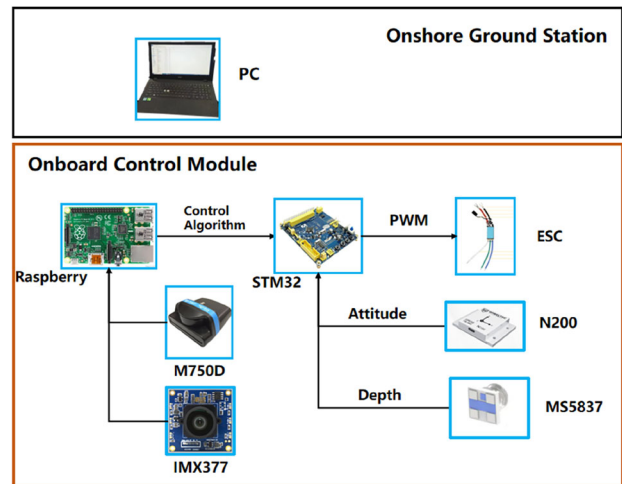
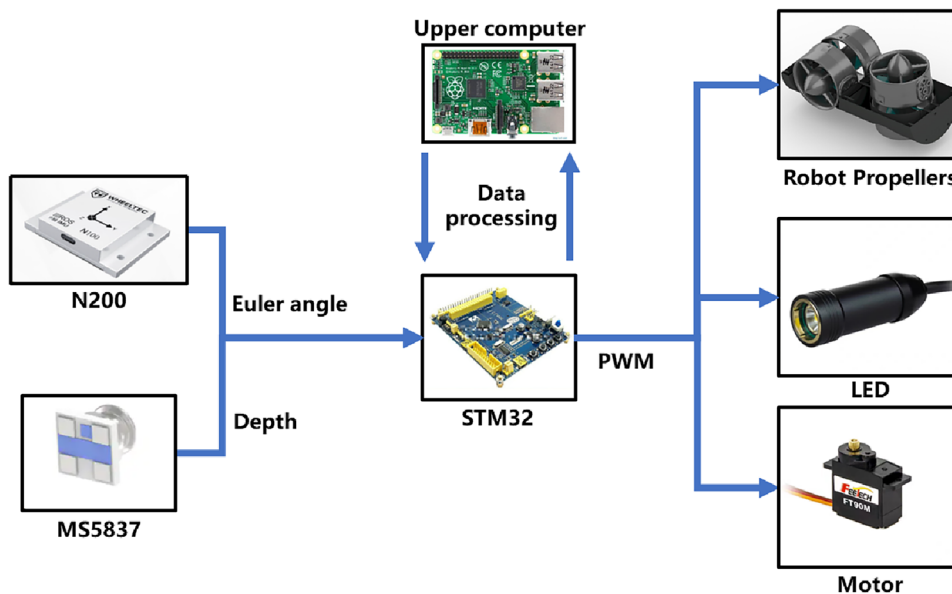


Fig. 7 Overall architecture of the control module

remotely control it via SSH protocol, with ROS’s distributed structure enabling data sharing between the two.

Fig. 8 The working process of STM32



Lower computer At the current stage, the STM32 development board in the snake-like robot primarily controls the rotational speed of the propellers at each joint, responding to PWM signal instructions based on commands from the upper computer. The MiniSTM32 development board (Zhengdian Atomic, China) is selected as the drive control board. The MiniSTM32 development board utilizes the STM32F103RBT6 as its MCU, operates at a frequency of 72 MHz, and allocates 8 timer channels to output PWM signals to the propellers. Additionally, a serial port interface is allocated for receiving data from the MS5837 depth sensor, and an IIC interface for receiving Euler angle data from the N200 nine-axis sensor. Furthermore, a USB serial port is allocated for communication with upper-level devices (Raspberry Pi), to transmit sensor data to the Raspberry Pi or to receive PWM data from it. The program is developed using Keil software, and the control process of STM32 is illustrated in Fig. 8.

Position sensors The MS5837 depth sensor (TECONNECTIVITY, China) and the N200 nine-axis attitude sensor (WHEELTEC, China) are utilized to measure the depth and attitude of the snake-like robot, respectively. The MS5837 depth sensor, equipped with a built-in solution board, calculates the depth signal and transmits it to the STM32 via serial communication. This setup allows the STM32 to directly receive and process the depth data without the need for additional calculations. Additionally, the N200 nine-axis attitude sensor is adopted, providing a more comprehensive data set compared to the MPU series of attitude sensors, as it includes three magnetometers, making it a 9-axis sensor. This enhancement ensures more accurate collection of the snake-like robot's attitude data, especially in terms of the

yaw angle ψ , where the N200, after applying a complementary filter algorithm, hardly experiences any drift. Overall, this data collection scheme for the snake-like robot's sensors is characterized by its simplicity, reliability, and precision, providing important data support for the control and navigation of the snake-like robot.

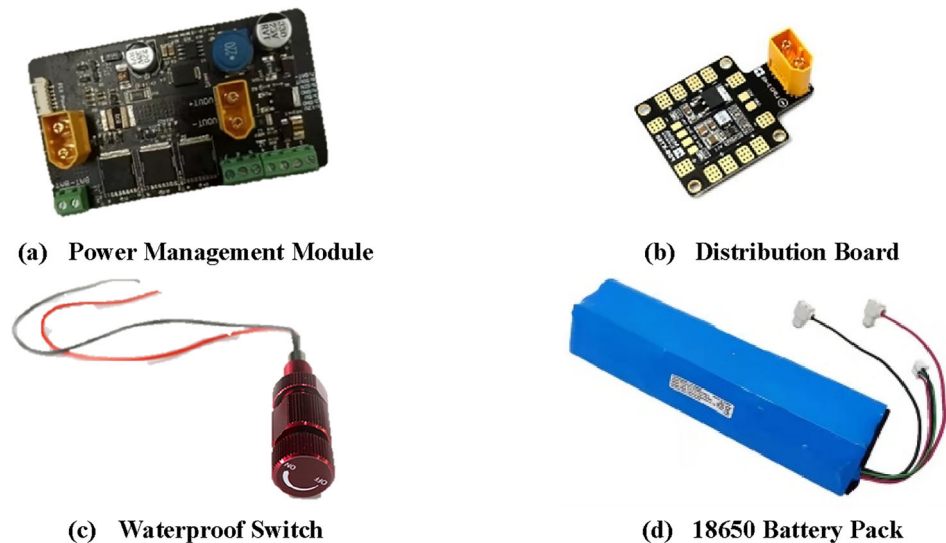
Power management module The hardware control system of the snake-like robot is powered by a 22 V 18650 model aircraft battery pack, necessitating efficient power distribution. The ROV marker power management module is adopted for managing and distributing the power. The model aircraft battery connects to the input of the power management module, while the outputs of the power management module are connected to two distribution boards. These distribution boards provide power to the propellers, Raspberry Pi, and STM32, respectively. Finally, the waterproof switch is connected to the power input of the power management module. The waterproof switch, distribution boards, and power management module are showcased in Fig. 9.

3.6.2 Operational modes

The underwater robot's control system provides users with a choice between two unique operational modes. In the remote-control mode, operators direct the robot using a ground terminal computer. Alternatively, in the autonomous patrol mode, the control module autonomously analyzes and broadcasts actuating signals.

Remote-control mode This mode emphasizes a seamless human-computer interface. Operators relay commands to

Fig. 9 Components of the snake-like robot



the robot's control module through a ground terminal. Concurrently, the robot gauges its motion using inputs from the attitude sensor, Doppler velocimeter, and a six-axis accelerometer. A Proportional-Integral (PI) algorithm then processes these inputs, factoring in the discrepancy between the desired and current attitudes, to generate a control signal. This signal is dispatched to both the propulsion system and the flexible joint module for execution.

For enhanced precision in motion attitude control, a predefined connecting rod model is utilized. Each module's tail has its own Cartesian coordinate system with two degrees of freedom, leading to overlapping coordinate system origins. Using data from the six-axis accelerometer in the cavity module, the rotation matrix between adjacent systems is determined. This facilitates the derivation of each module tail's relative motion attitude compared to its predecessor. By sequentially processing from the tail module, the motion attitude for every module's tail is ascertained, further aiding in control signal computation. These signals, mainly focused on adjusting to the desired attitude, directly modulate the flexible joint module's steering engine and the propulsion system's thrusters, ensuring the robot's accurate and responsive motion control.

Autonomous patrol In this mode, operators define a target using the ground computer. The control module then manages the propulsion system and the flexible joint module based on this target. Sensors continue to relay real-time data to the ground terminal via an ultrasonic communication unit throughout the task's execution.

The autonomous patrol mode's cornerstone is its automatic obstacle avoidance capability, heavily reliant on ultrasonic probes for distance measurement. The robot determines the optimal obstacle avoidance strategy by analyzing ultrasound distance measurements and its current motion attitude.

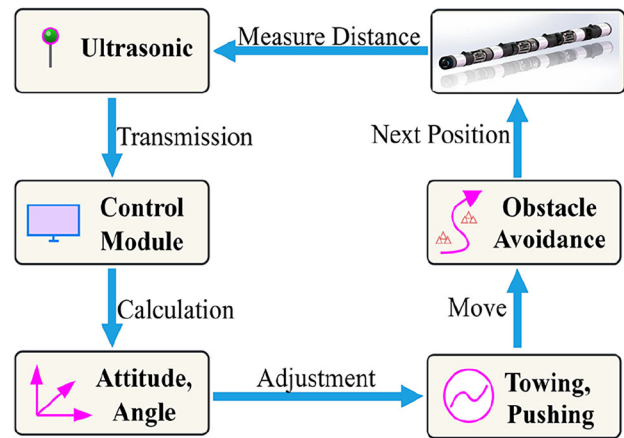


Fig. 10 The process of automatic obstacle avoidance function

This analysis informs the necessary attitude adjustments to navigate around obstacles, as illustrated in Fig. 10.

A primary design goal for this function is to maintain the structural integrity of the flexible underwater robot. When obstacles are detected via ultrasonic signals, the central processing unit evaluates the best movement and path for avoidance, simultaneously referencing the current motion attitude from the six-axis accelerometers. After determining the necessary attitude adjustments, which include parameters like orientation angles, the control module directs the propulsion system and the flexible joint module. Notably, the flexible joint module's steering engine modifies the robot's attitude based on the orientation angle, while the adjacent omnidirectional thruster module counter-rotates to navigate around obstacles.

3.7 Estimated operational duration analysis

In the current design, energy management is a critical factor in ensuring the effective and sustained operation of the serpentine underwater robot. A series of calculated steps have been taken to accurately assess the robot's energy consumption and estimated operational duration, ensuring that the robot has an adequate power supply while performing tasks.

Initially, detailed records of the power consumption of the thrusters in various operational states, including idle, low, medium, and high speeds, were compiled. Additionally, the power consumption of all sensors during operation was documented. Power consumption for other electrical components, such as controllers and communication modules, is also listed in Table 2.

Based on the anticipated operational state of the robot, the average power consumption has been calculated. This was achieved by multiplying the power consumption of each component by the percentage of total operational time it occupies, and then summing the results for all components. The formula is as follows:

$$P_{\text{avg}} = \sum (P_i \times T_{\text{percent}, i}) \quad (2)$$

where P_{avg} represents the average power consumption, P_i is the power consumption of the i th component, and $T_{\text{percent}, i}$ is the percentage of total operational time occupied by the i th component.

The serpentine robot is segmented into six distinct modules: the head, tail, five control modules, three flexible joint modules, two rotating head modules, and four omnidirectional thruster modules. Each control module is equipped with an N200 attitude sensor and an MS5837 depth sensor to ensure precise navigation and depth maintenance. The MiniSTM32 microcontroller orchestrates the coordination of these six modules through a bus system, eliminating the need for multiple controllers and thus optimizing energy efficiency.

The Raspberry Pi serves as the central processing unit, interfacing solely with the MiniSTM32. This streamlined communication means that only one Raspberry Pi is required for the entire robot, which, along with the camera, LED lights, and camera assembly, is housed within the head of the robot. The tail section contains a primary propulsion unit. Each flexible joint module operates with eight motors, and each omnidirectional thruster module contains two thrusters, further contributing to the robot's maneuverability. The rotating head modules are outfitted with sonar and a camera for environmental scanning and data acquisition.

During closed-loop control operations, the thrusters are not continuously active, allowing for a duty cycle (T_{percent}) of 0.5, which reduces energy consumption when full propulsion is not necessary. In contrast, other hardware components,

such as sensors and processing units, require constant operation, assigning them a T_{percent} of 1. Utilizing Table 2 and Eq. (2), the power consumption for each module can be calculated, along with the average power consumption for the entire robot. This approach ensures a comprehensive understanding of the robot's energy requirements, facilitating the optimization of its operational endurance and efficiency (Table 3).

The average power consumption for the robot design presented in this study is calculated to be 564.24 watts. As outlined in Table 2, the combined energy capacity of the battery set is 603.84 Wh. Operational duration is derived by dividing the total battery capacity by the average power demand, resulting in an estimated operational time of approximately 1.07 h for the current design. To prevent the robot from shutting down due to battery exhaustion during essential operations, a safety factor is integrated into the operational time calculation. The adjusted operational time, with the safety factor taken into account, is calculated as follows:

$$T_{\text{safe}} = T_{\text{work}} \times (1 - \text{SF}) \quad (3)$$

Here the safety factor (SF) is chosen to be 0.2. This value strikes a balance between providing a sufficient energy buffer and avoiding an overly conservative limitation on the robot's total operational period.

With these calculations, the anticipated operational time for the serpentine underwater robot designed in this research is established at 60 min. This represents a strategic and pragmatic approach to energy management, designed to ensure sustained and stable functionality in subaquatic conditions.

4 Motion control

4.1 Kinematics of the flexible joint

Figure 11 depicts the flexible joint, which, when constructed with multiple springs, can be likened to a flexible link. During the operation of the underwater robot, this link experiences two primary orthogonal forces:

- F_1 : the axial thrust that aligns with the omnidirectional thruster module.
- F_2 : a thrust that is perpendicular to the axis of the omnidirectional thruster module.

Additional forces, F_3 and F_4 , act orthogonally on the adjacent flexible link. F_u , F_v and F_w signify the cumulative forces exerted by the other modules on the flexible link, projected onto a 3D coordinate system. The origin of this system is situated at the end of the flexible joint that connects to the

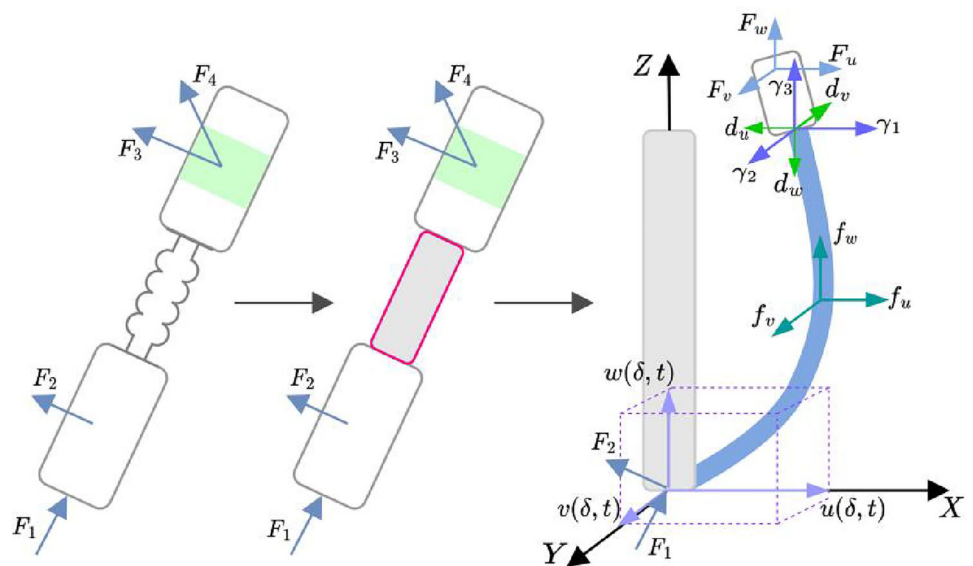
Table 2 Hardware information utilized in this design

Unit	Model	Parameters	Manufacturer information
Upper computer	Raspberry Pi 4B	Storage space: 8G PAM + 32 G Memory card Voltage: 5 V Current: 3 A	Raspberry Pi Foundation, U.K
Lower computer	MiniSTM32	MCU: STM32F103RBT6 Operating frequency: 72 MHz Voltage: 5 V	Zhengdian Atomic Technology Co. Ltd, China
Propeller	P75	Maximum Forward Thrust: 6.2 kg Maximum Reverse Thrust: 4.5 kg Voltage: 10–30 V Current: 2.5–13.1 A	HYDROCEAN, China
Attitude sensor	Nine-axis N200	Three-axis gyroscope Three-axis accelerometer Three-axis magnetometer Voltage: 5 V Current: < 40 mA	WHEELTEC, China
Depth sensor	MS5837	Pressure range: 30,000 mbar Output: 24-bit ADC Voltage: 1.5–3.6 V	TECONNECTIVITY, China
Sonar	M750D	Exploration distance: 120 m/40 m Voltage: 12–48 V Current: 0.5–1.3 A	OCEANXER, China
Camera	IMX377	IMX277 12M 1/2.3 1.55 44 SLVS-EC 8Lane Voltage: 5 V	Shenzhen Lingwo Precision Technology Development Co. Ltd, China
Battery	18,650 Battery pack	Capacity: 27.2 Ah/603.84 wh	Battewill, China
Power management module	ROV marker	Input: 27.2 V Output: 5 V/12 V	ROVmarker, China
Power distribution board	XT60	Input: 27.2 V Output: 12 V	ROVmarker, China
LED	ELEC-L1200-15	Input: 12–28 V Power: 15(Max)	Ocean Technology, China
Steering engine	FT90M	Input: 4.8 V 800 mA Torque force: 2 kg	FEETECH RC Model Co, China
Switch	M10	Operating voltage: 125 VAC Operating current: 0.5 A	ROVmarker, China

Table 3 Power consumption of snake robot

Distinct modules	Module amount	Unit	Unit amount	P_i
Head module	1	Upper computer	1	$P_{11} = 5V * 3A = 15W$
		Lower computer	1	$P_{12} = 5V * 1A = 5W$
		LED	1	$P_{13} = 5V * 2A = 10W$
		Camera	1	$P_{14} = 5V * 0.1A = 0.5W$
Power consumption P_1				$P_1 = P_{11} + P_{12} + P_{13} + P_{14} = 30.5W$
Tail module	1	Main propeller	1	$P_{21} = 20V * 6A * 0.5 = 60W$
Power consumption P_2				$P_2 = P_{21} = 60W$
Control module	5	Attitude sensor	1	$P_{31} = 5V * 0.04A = 0.2W$
		Depth sensor	1	$P_{32} = 3.6V * 0.01A = 0.036W$
Power consumption P_3				$P_3 = P_{31} * 5 + P_{32} * 5 = 1.18W$
Rotating head modules	2	Camera	1	$P_{41} = 5V * 0.04A = 0.2W$
		Sonar	1	$P_{42} = 30V * 1A = 30W$
Power consumption P_4				$P_4 = P_{41} * 2 + P_{42} * 2 = 60.4W$
Flexible joint module	3	Steering engine	8	$P_{51} = 4.8V * 0.8A * 8 = 30.72W$
Power consumption P_5				$P_5 = 3 * P_{51} = 92.16W$
Omnidirectional thruster module	4	Propeller	2	$P_{61} = 20V * 4A * 2 * 0.5 = 80W$
Power consumption P_6				$P_6 = 4 * P_{61} = 320W$
Average power consumption P_{avg}				564.24W

Fig. 11 Equivalent flexible link diagram



omnidirectional thruster module. The X – Y plane of this system represents the cross-section of the flexible joint, with the z -axis indicating its neutral axis. The variables $u(\delta, t)$, $v(\delta, t)$, and $w(\delta, t)$ denote the three linear displacements. Meanwhile, f_u , f_v , and f_w represent the forces due to the flow on the link. Other variables like d_u , d_v , and d_w account for the nonlinear disturbances at the link's end, and γ_1 , γ_2 , and γ_3 are the control inputs from the link's end-effector.

The motion dynamics of this equivalent flexible link are captured in n Eqs. (4) to (6) [36, 37], and the definition of the mathematical symbols are described in Table 4:

$$m_0 \ddot{u} = -EIu_{\delta\delta\delta\delta} + \left(F_{\vartheta} + \frac{3}{2}EAu_{\delta}^2 \right) u_{\delta\delta} + EA(u_{\delta}w_{\delta\delta} + u_{\delta\delta}w_{\delta}) + \frac{EA}{2}(u_{\delta\delta}v_{\delta}^2 + 2u_{\delta}v_{\delta}v_{\delta\delta}) + f_u \quad (4)$$

$$m_0 \ddot{v} = -EIv_{\delta\delta\delta\delta} + \left(F_{\vartheta} + \frac{3}{2}EAu_{\delta}^2 \right) v_{\delta\delta} + EA(v_{\delta}w_{\delta\delta} + v_{\delta\delta}w_{\delta}) + \frac{EA}{2}(v_{\delta\delta}u_{\delta}^2 + 2v_{\delta}u_{\delta}u_{\delta\delta}) + f_v \quad (5)$$

$$m_0 \ddot{w} = EA(w_{\delta\delta} + u_{\delta}u_{\delta\delta} + v_{\delta}v_{\delta\delta}) + f_w \quad (6)$$

Equation (4) describes the kinetic equation for the u displacement, incorporating factors like bending stiffness, axial force, and the elastic modulus. Equation (5) similarly describes the kinetic equation for the v displacement, while Eq. (6) focuses on the w displacement.

In these equations, m_0 represents the sum of the unit mass (ρA) of the link and its additional mass (m_a). EI denotes its bending stiffness, EA represents the product of the elastic modulus, and F_{ϑ} is the axial force acting on the flexible link.

Given that the length of an equivalent flexible link is L , it must adhere to specific boundary conditions, as outlined in Eqs. (7) to (9).

$$\gamma_1 + F_u + d_u = -EIu_{\delta\delta\delta\delta}(L) + F_{\vartheta}u_{\delta}(L) + \frac{EA}{2} \left[u_{\delta}^3(L) + u_{\delta}(L)v_{\delta}^2(L) + 2w_{\delta}u_{\delta} \right] \quad (7)$$

$$\gamma_2 + F_v + d_v = -EIv_{\delta\delta\delta\delta}(L) + F_{\vartheta}v_{\delta}(L) + \frac{EA}{2} \left[v_{\delta}^3(L) + v_{\delta}(L)u_{\delta}^2(L) + 2w_{\delta}v_{\delta} \right] \quad (8)$$

$$\gamma_3 + F_w + d_w = F_{\vartheta} + EAu_{\delta}(L) + \frac{EA}{2} \left[u_{\delta}^2(L) + v_{\delta}^2(L) \right] \quad (9)$$

Furthermore, the structure of the equivalent flexible link must also satisfy initial conditions, as presented in Eqs. (10–13).

$$u(0, t) = v(0, t) = w(0, t) = 0 \quad (10)$$

Table 4 Definition of mathematical terms

Symbol	Description
m_0	Mass of the flexible joint
EI	Bending stiffness
A	Cross-sectional area of the equivalent flexible rod
$u(\delta, t)$	Offset of the flexible joint on the x axis
\ddot{u}	Second-order derivative of the offset on the x axis with respect to time
u_{δ}	First-order derivative of the flexible joint offset with respect to x
$u_{\delta\delta}$	Second-order derivative of the flexible joint offset with respect to x
$u_{\delta\delta\delta\delta}$	Fourth-order derivative of the flexible joint offset with respect to x
$v(\delta, t)$	Offset of the flexible joint on the y axis
\ddot{v}	Second-order derivative of the offset on the y axis with respect to time
v_{δ}	First-order derivative of the flexible joint offset with respect to y
$v_{\delta\delta}$	Second-order derivative of the flexible joint offset with respect to y
$v_{\delta\delta\delta\delta}$	Fourth-order derivative of the flexible joint offset with respect to y
$w(\delta, t)$	Offset of the flexible joint on the z axis
\ddot{w}	Second-order derivative of the offset on the z axis with respect to time
w_{δ}	First-order derivative of the flexible joint offset with respect to z
$w_{\delta\delta}$	Second-order derivative of the flexible joint offset with respect to z
$w_{\delta\delta\delta\delta}$	Fourth-order derivative of the flexible joint offset with respect to z
F_{ϑ}	Axial force acting on the equivalent flexible rod
f_u, f_v and f_w	Underwater current disturbances acting as three component forces on the flexible rod
F_u, F_v and F_w	Three component forces exerted by other structures on the flexible rod
d_u, d_v and d_w	Nonlinear disturbances acting at the end of the flexible joint

$$v_{\delta\delta}(0, t) = v_{\delta\delta}(L, t) = 0 \quad (11)$$

$$u_{\delta\delta}(0, t) = u_{\delta\delta}(L, t) = 0 \quad (12)$$

$$F_u(0, t_0) = F_{u0}, F_v(0, t_0) = F_{v0}, F_w(0, t_0) = F_{w0} \quad (13)$$

By employing this comprehensive set of equations, one can iteratively compute the linear displacements at both ends

of a flexible joint, allowing for a deeper understanding of the joint’s motion dynamics.

4.2 Kinematics of the snake-like robot

The exact positioning of the ends of each module group is vital for controlling a multi-joint robot’s movement during its standard operation. The snake-like robot’s motion model is built upon a multi-coordinate framework. As illustrated in Fig. 12, there are eight coordinate systems, specifically z_1 to z_8 , established at each flexible joint’s end. In addition, there’s a foundational zero-coordinate system, z_0 , and a tool-coordinate system, z_8 . Every z -axis is in alignment with the linkage axis direction. The associated x -axis runs perpendicular to the z -axis within the graphical plane, and the y -axis is determined using the right-hand rule.

Positioning sensors, integrated into the control mode, are essential for determining the Euler angles of each joint’s posture during the robot’s operation. It is postulated that the current coordinate system has undergone rotations of r , p and h degrees around the z -axis, x -axis and y -axis, respectively, from its prior state. The rotation transformation matrix can be expressed as:

$$\text{Eul}(r, p, h) = \begin{bmatrix} c_r c_h - s_r s_p s_h & -s_r c_p & c_r s_h + s_r s_p c_h \\ s_r c_h + c_r s_p & s_h c_r & c_p s_r s_h - c_r s_p c_h \\ -c_p s_h & s_p & c_p c_h \end{bmatrix} \tag{14}$$

While the positions of the flexible joints in each coordinate system can be deduced using Eqs. (4) to (13), determining the spring’s end position remains theoretically challenging due to its bending nature and the variance between the distance of its ends and its resting length. However, given the infinite degrees of freedom of an equivalent flexible link, the posture sensor can gauge the spring’s end position. The transformation matrices between the coordinate systems, leveraging the Euler angle data from the posture sensor and Eq. (14), are represented as:

$$\begin{cases} {}^0_1T = \begin{bmatrix} \text{Eul}(r_1, p_1, h_1) & 0 \\ 0 & 1 \end{bmatrix}, & {}^1_2T = \begin{bmatrix} I & J_1 \\ 0 & 1 \end{bmatrix} \\ {}^2_3T = \begin{bmatrix} \text{Eul}(r_2, p_2, h_2) & J_2 \\ 0 & 1 \end{bmatrix}, & {}^3_4T = \begin{bmatrix} I & J_3 \\ 0 & 1 \end{bmatrix} \\ {}^4_5T = \begin{bmatrix} \text{Eul}(r_3, p_3, h_3) & J_4 \\ 0 & 1 \end{bmatrix}, & {}^5_6T = \begin{bmatrix} I & J_5 \\ 0 & 1 \end{bmatrix} \\ {}^6_7T = \begin{bmatrix} \text{Eul}(r_4, p_4, h_4) & J_6 \\ 0 & 1 \end{bmatrix}, & {}^7_8T = \begin{bmatrix} I & J_7 \\ 0 & 1 \end{bmatrix} \end{cases} \tag{15}$$

Here, I stands for an identity matrix. J_2 , J_4 and J_6 are presumed to be the coordinate values of L_2 , L_4 , and L_6 at the

axes of z_2 , z_4 and z_6 , respectively. The computation formula is:

$$\begin{cases} J_2 = [u_1(L_2)v_1(L_2)w_1(L_2)1]^T \\ J_4 = [u_2(L_4)v_2(L_4)w_2(L_4)1]^T \\ J_6 = [u_3(L_6)v_3(L_6)w_3(L_6)1]^T \end{cases} \tag{16}$$

Similarly, $J_i = [0 \ 0 \ L_i \ 1]^T$, where i belongs to [1, 3, 5, 7]. Subsequently, the tool-coordinate system’s position in the zero-coordinate system is depicted in Eq. (17). This allows for the extraction of the robot’s head model motion characteristics within an absolute coordinate system.

$${}^0_8T = \prod_{k=1}^8 {}^k_{k-1}T = \begin{bmatrix} n_1 & o_1 & a_1 & \xi_1 \\ n_2 & o_2 & a_2 & \xi_2 \\ n_3 & o_3 & a_3 & \xi_3 \\ 0 & 0 & 0 & 1 \end{bmatrix} = \begin{bmatrix} {}^0_8R & \xi \\ 0 & 1 \end{bmatrix} \tag{17}$$

5 Experimental investigation of the flexible joints

Traditional underwater robots typically employ rigid connections to link their components, which may restrict movement in complex underwater environments. The integration of flexible joints can significantly enhance a robot’s agility, allowing for more adaptable and fluid motion in response to varying conditions, such as water currents and waves. To substantiate the efficacy of the proposed underwater snake-like robot, a comprehensive set of simulations and comparative analyses was undertaken in this research, with a particular focus on how flexible joints can expand the robot’s operational workspace.

5.1 Experimental setup

5.1.1 Finite element model design

The finite element model (FEM) of the flexible joint was developed to conduct a comprehensive mechanical analysis, simulating the forces and deformations experienced by the joint. The design of the model was based on an in-depth analysis of the bending characteristics and other physical properties of the flexible joints used in the robot design, effectively represented as flexible rod models in the simulation.

To accurately replicate the behavior of the flexible joints, the model was assigned a Poisson’s ratio of 0.45, with three different elastic moduli and four different lengths of the flexible rods used to simulate the equivalent flexible joints

Fig. 12 Multi-coordinate framework of the snake-like robot

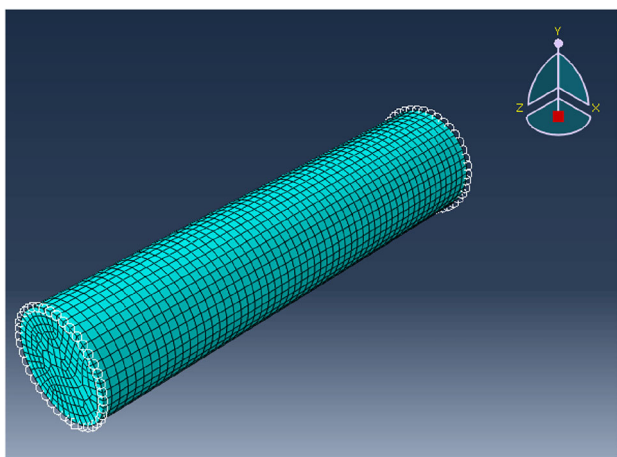
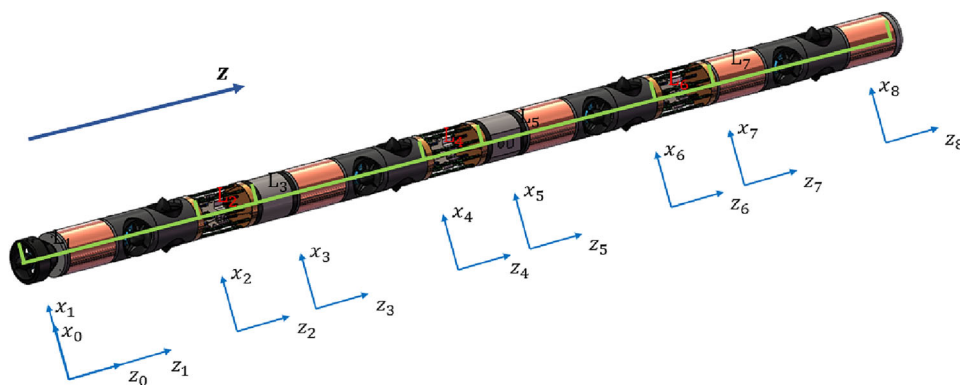


Fig. 13 Finite element model of the equivalent flexible joint

under various conditions. The simulation employed three-dimensional solid elements and eight-node linear hexahedral elements, with a mesh size of 9 mm.

The finite element model of the equivalent flexible joint, depicted in Fig. 13, is crucial for understanding the simulation setup and interpreting the results. By varying the elastic modulus and the length of the flexible rods, the experiment simulated the robot's movement under different working conditions, allowing for a direct comparison between the performance of rigid connection units and various types of flexible joint units in an underwater environment.

The experiment provided quantitative data on the end displacement of the connecting units, the displacement angles, and an analysis of the working space. The working space analysis is significant as it provides insights into the range of motion and flexibility that the flexible joints offer compared to rigid connections. This information is vital for optimizing the robot's design for specific underwater tasks, ensuring effective navigation and operation in complex underwater terrains.

Additionally, the FEM allowed for the assessment of the flexible joints' structural integrity under simulated underwater currents and pressures. By applying different forces

and boundary conditions to the model, the study evaluated the joints' resilience and the potential for material fatigue or failure.

Overall, the finite element analysis of the flexible joints provides a detailed understanding of their mechanical behavior, essential for the design and development of advanced serpentine underwater robots. The ability to predict the performance of these joints under various conditions ensures that the robot can be reliably deployed in challenging underwater environments, performing tasks with the required precision and flexibility.

5.1.2 Boundary conditions

In this design, the modules of the underwater robot are interconnected through flexible joints. The boundary conditions applied at the ends of the equivalent flexible rod include the gravity, buoyancy, and motor thrust of the different modules connected by the flexible joints. Regarding gravity and buoyancy, the design of the underwater robot has already accounted for weight adjustment in different water density environments to achieve neutral buoyancy of the robot modules, meaning the combined force of gravity and buoyancy is zero, allowing for autonomous suspension of the robot modules. Therefore, in this experiment, the effects of gravity and buoyancy will not be considered, and the focus of the boundary conditions will be on motor thrust.

The selection of the motor is crucial for the proper functioning of the flexible joints. The ends of the flexible joints are controlled by the motor to reach predetermined positions. During this process, whether the flexible joint can function properly depends on its own elastic modulus and the thrust provided by the motor. If the thrust provided by the motor is insufficient, the displacement at the end of the flexible rod will be small, failing to reach the intended position. In this experiment, the chosen motor can deliver a maximum torque of 60 Newtons (N), which acts directly on the end of the flexible joint.

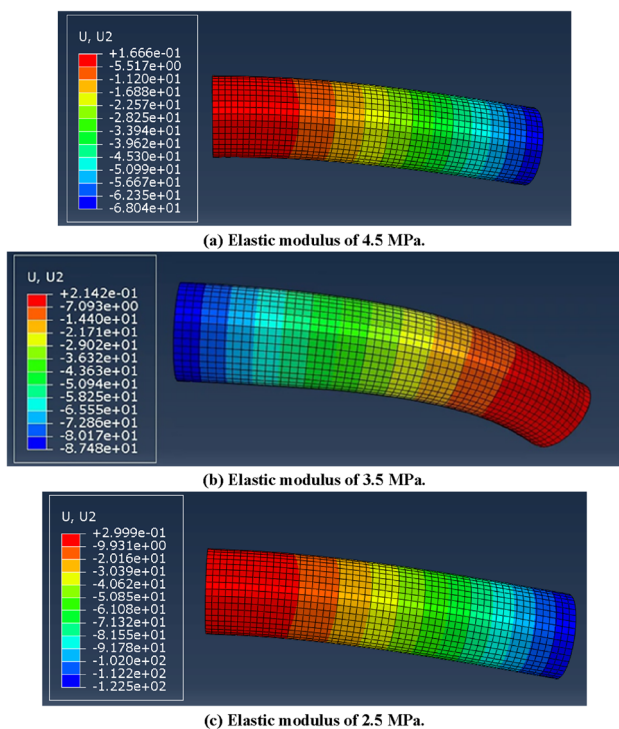


Fig. 14 Finite element analysis of equivalent flexible joints with different elastic moduli

With such a setup, the experiment can accurately simulate the impact of motor thrust on the performance of the flexible joints, thereby providing important data support for the design and operation of the underwater robot.

5.2 Numerical simulation results

This study focuses on the impact of different flexible joints on the functionality of an underwater serpentine robot, particularly how the elastic modulus of the joints affects the robot’s operation. The flexible joints of the robot are characterized by an equivalent elastic modulus of 3.5 MPa and a rod length of 156 mm. Under maximum motor power conditions, the end displacement of the flexible joint reaches 87.48 mm, which corresponds to a maximum end displacement angle of approximately 30°, as determined by trigonometric analysis.

The experiment first examined the changes in end displacement of the flexible joint when the equivalent elastic modulus was set at 2.5 MPa and 4.5 MPa. As depicted in Fig. 14, with an elastic modulus of 4.5 MPa, the end displacement of the flexible joint was only 68.04 mm, resulting in a displacement angle of 23.5°. In contrast, a flexible joint with an elastic modulus of 2.5 MPa achieved an end displacement of 122.50 mm and an angle of 38°. While a lower elastic modulus allows for a farther end position and a larger working space, it also results in lower disturbance resistance due to the material properties, making it challenging to control

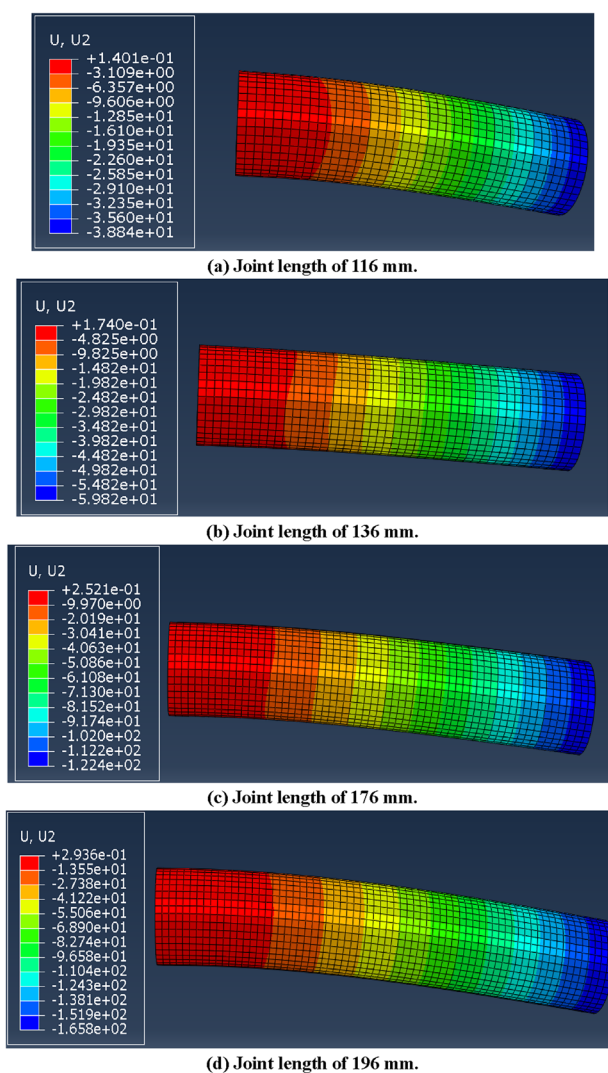


Fig. 15 Finite element analysis of flexible joints of different lengths with an elastic modulus of 3.5 MPa

the joint accurately in underwater conditions like turbulence. Conversely, a higher elastic modulus enhances the joint’s stability but limits the end position it can reach. Therefore, the production of flexible joints should consider an appropriate equivalent elastic modulus to balance stability and working space size.

In addition to the elastic modulus, the study also explored the effect of the length of the flexible joints on the robot. With the equivalent elastic modulus fixed at 3.5 MPa, the experiment compared the end displacements and angles for lengths of 116 mm, 136 mm, 176 mm, and 196 mm. The results, shown in Fig. 15 and Table 5, indicate that longer flexible joints typically allow for a greater range of motion, expanding the working space and enabling adaptation to narrow passages or complex underwater environments. However, this also introduces more complex control issues, as the flexure and deformation of the joints must be considered to maintain

Table 5 End displacement and displacement angles for different lengths of flexible joints

Joint length (mm)	Displacement (mm)	Displacement angle (degrees)
116	38.8	18.5
136	59.8	23.7
156	87.5	29.8
176	122.4	34.8
196	165.8	40.2

the required shape and posture. Additionally, longer joints may lead to instability and oscillation at high speeds or under heavy loads. They may also require more energy to control and maintain their shape, increasing the robot's energy consumption. Thus, the length of the flexible joints should be optimized and selected based on specific tasks and application requirements to ensure that the underwater serpentine robot can perform tasks stably and efficiently in its working environment.

To highlight the benefits of flexible joints in augmenting the workspace and agility of soft-bodied robots, this study meticulously contrasted the workspace boundaries of flexible joints with those of conventional rigid connections through finite element simulation. The methodology entailed replacing flexible joints with rigid ones to assess the maximal extent each could reach within the same horizontal plane. Figure 16a illustrates the workspace limitations of a conventional rigid connection upon motor fixation. Here, structural constraints impose restrictions on full rotational movement, confining the motion to the same plane as the motor. In contrast, Fig. 16b delineates the boundary of the workspace for a flexible connection, showcasing its capability for full rotational motion and operation across multiple planes.

Flexible joints impact the operational workspace of underwater serpentine robots in several ways. Primarily, they extend the workspace, granting the robot increased degrees of freedom and flexibility to navigate complex, narrow, or otherwise inaccessible areas. This enhancement boosts the robot's maneuverability and adaptability in underwater settings, allowing it to conform to irregular surfaces and serpentine paths. However, the introduction of flexible joints also brings the complexity of dynamic control into play, necessitating sophisticated algorithms and sensors to accommodate environmental variations and flexural movements, thereby posing challenges in system design and control. In summary, the design of flexible joints also contributes to the robot's adaptability in aquatic environments and mitigates the risk of collision damage. Therefore, when designing and operating underwater serpentine robots, it is crucial to balance the effects of elastic modulus and workspace to

maximize the advantages of flexible joints. Future research should consider incorporating more comprehensive sensors and developing robust control algorithms to achieve stable management of flexible joints.

6 Conclusion

This paper provides an in-depth analysis of the design, structure, and functional capabilities of a biomimetic underwater snake-like robot, highlighting several key aspects and innovations:

- *Biomimetic design* the study elaborates on the biomimetic framework of the robot, inspired by the physiological mechanisms of snakes. This approach is pivotal as it enhances the robot's navigational and operational proficiency in multifaceted aquatic environments.
- *Modular architecture* the robot boasts a modular configuration, incorporating an array of sensors, omnidirectional propulsion units, and flexible joints. This modular strategy augments the robot's versatility and efficiency in executing diverse subaquatic missions.
- *Control module* the paper delves into the intricate design and potential of the control module. The control tactics are fine-tuned for motion management, a vital element for the robot's precision and effectiveness in submerged conditions.
- *Simulation experiments* results from finite element simulation experiments are presented, providing essential insights into the robot's performance metrics in comparison to conventional systems. These findings highlight the advantageous impact of the robot's flexible joints on its agility and maneuverability.
- *Sensing systems* the robot is outfitted with a dual sensing mechanism, comprising navigational sensors for environmental perception and diagnostic sensors for assessing the integrity of subsea structures. This dual capability is crucial for the robot's deployment in surveillance and inspection operations.
- *Future work* the study outlines potential directions for future research, underscoring its contribution to the progressive field of underwater robotics and the prospects for further technological breakthroughs.

In conclusion, this research represents a leap in underwater robotics, merging biomimetic design with cutting-edge engineering practices. The serpentine robot is a testament to progress in the domain, enhancing the scope for aquatic exploration and structural health monitoring. Its modular architecture, combined with an advanced control system and extensive sensor networks, empowers the robot to undertake

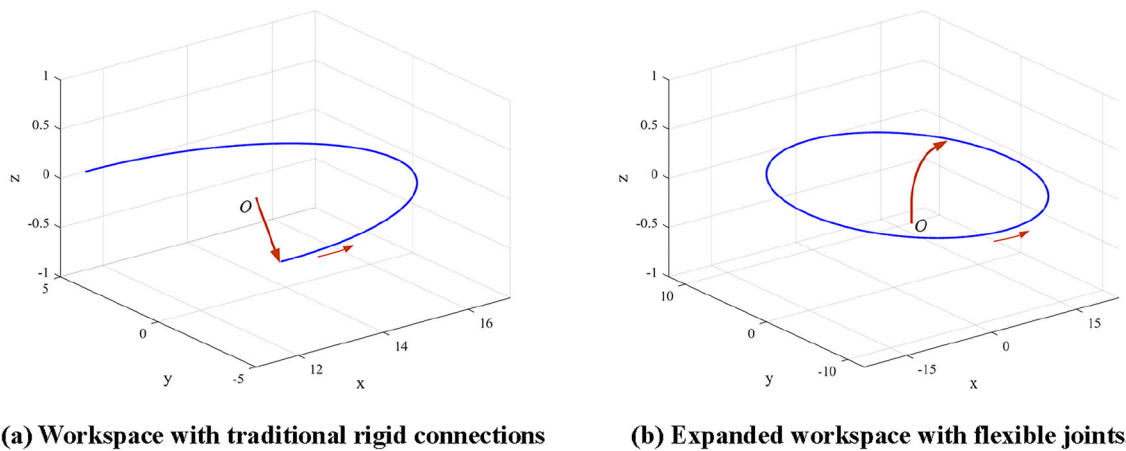


Fig. 16 Workspace range comparison: flexible joints versus traditional rigid connections

intricate tasks in demanding underwater scenarios. The presented research not only demonstrates current capabilities but also paves the way for future advancements in robotic technologies for underwater applications. The comprehensive simulation studies and discussions on the robot's potential uses emphasize its practical significance and its contributions to the robotics industry.

Funding This paper was supported by the Guangzhou Basic Research Program Jointly Funded by Municipal Schools (Institutes) and Enterprises (No. 2024A03J0318), National key R&D plan (NO. 2022YFB2603303), the Technology Planning Project of Guangzhou City (No. 20212200004), 111 Project (No. D21021).

Declarations

Conflict of interest The authors have no relevant financial or non-financial interests to disclose.

Open Access This article is licensed under a Creative Commons Attribution 4.0 International License, which permits use, sharing, adaptation, distribution and reproduction in any medium or format, as long as you give appropriate credit to the original author(s) and the source, provide a link to the Creative Commons licence, and indicate if changes were made. The images or other third party material in this article are included in the article's Creative Commons licence, unless indicated otherwise in a credit line to the material. If material is not included in the article's Creative Commons licence and your intended use is not permitted by statutory regulation or exceeds the permitted use, you will need to obtain permission directly from the copyright holder. To view a copy of this licence, visit <http://creativecommons.org/licenses/by/4.0/>.

References

1. Yang X, Zheng L, Lü D, Wang J, Wang S, Su H, Wang Z, Ren L (2022) The snake-inspired robots: a review. *Assem Autom* 42(4):567–583. <https://doi.org/10.1108/AA-03-2022-0058>
2. Costa D, Palmieri G, Palpacelli M-C et al (2018) Design of a bio-inspired autonomous underwater robot. *J Intell Robot Syst* 91:181–192. <https://doi.org/10.1007/s10846-017-0678-3>
3. Youssef SM, Soliman M, Saleh MA et al (2022) Underwater soft robotics: a review of bioinspiration in design, actuation, modeling, and control. *Micromachines* 13:110. <https://doi.org/10.3390/mi13010110>
4. Ahmadi A, Asgari M (2021) Novel bio-inspired variable stiffness soft actuator via fiber-reinforced dielectric elastomer, inspired by Octopus bimaculoides. *Intell Serv Robot* 14:691–705. <https://doi.org/10.1007/s11370-021-00388-1>
5. Chen G, Ti X, Shi L, Hu H (2022) Design of beaver-like hind limb and analysis of two swimming gaits for underwater narrow space exploration. *J Intell Robot Syst* 104:65. <https://doi.org/10.1007/s10846-022-01610-7>
6. Mori M, Hirose S (2002) Three-dimensional serpentine motion and lateral rolling by active cord mechanism ACM-R3. In: *Proceedings of the IEEE/RSJ International Conference on Intelligent Robots and Systems, Lausanne, Switzerland*, pp 829–834
7. Hirose S, Yamada H (2009) Snake-like robots [Tutorial]. *IEEE Robot Automat Mag* 16:88–98. <https://doi.org/10.1109/MRA.2009.932130>
8. Hirose S, Mori M (2004) Biologically inspired snake-like robots. In: *Proceedings 2004 IEEE International Conference on Robotics and biomimetics, Shenyang, China*, pp 1–7
9. Tadakuma K (2006) Tetrahedral mobile robot with novel ball shape wheel. In: *Proceedings of the first IEEE/RAS-EMBS International conference on biomedical robotics and biomechatronics, BioRob, Pisa, Italy*, pp 946–952
10. Kakogawa A, Komurasaki Y, Ma S (2019) Shadow-based operation assistant for a pipeline-inspection robot using a variance value of the image histogram. *J Robot Mechatron* 31:772–780. <https://doi.org/10.20965/jrm.2019.p0772>
11. Wright C, Johnson A, Peck A et al (2007) Design of a modular snake robot. In: *Proceedings of 2007 IEEE/RSJ International Conference on intelligent robots and systems, San Diego, CA, USA*, pp 2609–2614
12. Yu S, Ma S, Li B, Wang Y (2011) An amphibious snake-like robot with terrestrial and aquatic gaits. In: *Proceedings of 2011 IEEE International Conference on Robotics and Automation, Shanghai, China*, pp 2960–2961
13. Yu S, Ma S, Li B, Wang Y (2009) An amphibious snake-like robot: design and motion experiments on ground and in water. In: *Proceedings of 2009 International Conference on Information and Automation, Zhuhai/Macau, China*, pp 500–505

14. Rollinson D, Choset H (2016) Pipe network locomotion with a snake robot. *J Field Robot* 33:322–336. <https://doi.org/10.1002/rob.21549>
15. Hu DL, Nirody J, Scott T, Shelley MJ (2009) The mechanics of slithering locomotion. *Proc Natl Acad Sci USA* 106:10081–10085. <https://doi.org/10.1073/pnas.0812533106>
16. Crespi A, Badertscher A, Guignard A, Ijspeert AJ (2005) AmphiBot I: an amphibious snake-like robot. *Robot Auton Syst* 50:163–175. <https://doi.org/10.1016/j.robot.2004.09.015>
17. Crespi A, Ijspeert AJ (2006) AmphiBot II: an amphibious snake robot that crawls and swims using a central pattern generator. Brussels, Belgium, p 10
18. Liljebäck P, Stavdahl O, Pettersen KY, Gravadahl JT (2014) Mamba—a waterproof snake robot with tactile sensing. In: Proceedings of 2014 IEEE/RSJ International Conference on Intelligent Robots and Systems, Chicago, IL, USA, pp 294–301
19. Klaassen B, Paap KL (1999) GMD-SNAKE2: a snake-like robot driven by wheels and a method for motion control. In: Proceedings of 1999 IEEE International Conference on robotics and automation, Detroit, MI, USA, pp 3014–3019
20. Borenstein J, Hansen M, Borrell A (2007) The OmniTread OT-4 serpentine robot—design and performance. *J Field Robot* 24:601–621. <https://doi.org/10.1002/rob.20196>
21. Borenstein J, Borrell A (2008) The OmniTread OT-4 serpentine robot. In: Proceedings of 2008 IEEE International Conference on robotics and automation, Pasadena, CA, USA, pp 1766–1767
22. Siegwart R (2021) Worm-like softrobot for search and rescue missions focus project, Final Report, 122
23. Kelasidi E, Liljebäck P, Pettersen KY, Gravadahl JT (2016) Innovation in underwater robots: biologically inspired swimming snake robots. *IEEE Robot Automat Mag* 23:44–62. <https://doi.org/10.1109/MRA.2015.2506121>
24. Crespi A, Badertscher A, Guignard A, Ijspeert AJ (2005) Swimming and crawling with an amphibious snake robot. In: Proceedings of 2005 IEEE International Conference on robotics and automation, Barcelona, Spain, pp 3024–3028
25. Liljebäck P, Mills R (2017) Eelume: a flexible and subsea resident IMR vehicle. In Proceedings of OCEANS 2017—Aberdeen, Aberdeen, United Kingdom, pp 1–4
26. KONGSBERG EELY500-Articulated Underwater Robot, Eelume. Available: <https://www.kongsberg.com/globalassets/maritime/km-products/product-documents/eelume---underwater-intervention-vehicle>
27. Biorobotics Laboratory, Hardened Underwater Modular Robot Snake (HUMRS). Available: <http://biorobotics.ri.cmu.edu/robots/UnderWaterSnakeHUMRS.php>
28. Tang J, Li B, Li Z, Chang J (2017) A novel underwater snake-like robot with gliding gait. In: Proceedings of 2017 IEEE 7th Annual International Conference on CYBER technology in automation, control, and intelligent systems (CYBER), Honolulu, HI, pp 1113–1118
29. Gray J (1946) The mechanism of locomotion in snakes. *J Exp Biol* 23:101–120. <https://doi.org/10.1242/jeb.23.2.101>
30. Jian X, Zou T (2022) A review of locomotion, control, and implementation of robot fish. *J Intell Robot Syst* 106:37. <https://doi.org/10.1007/s10846-022-01726-w>
31. Graham JB, Lowell WR, Rubinoff I, Motta J (1987) Surface and subsurface swimming of the sea snake *Pelamis Platurus*. *J Exp Biol* 127(1):27–44. <https://doi.org/10.1242/jeb.127.1.27>
32. Boyer F, Porez M, Khalil W (2006) Macro-continuous computed torque algorithm for a three-dimensional eel-like robot. *IEEE Trans Robot* 22:763–775. <https://doi.org/10.1109/TRO.2006.875492>
33. Takanashi N, Chose H, Burdick JW (1993) Simulated and experimental results of dual resolution sensor based planning for hyper-redundant manipulators. In: Proceedings of 1993 IEEE/RSJ International Conference on intelligent robots and systems (IROS '93), Yokohama, Japan, pp 636–643
34. Linnemann R, Paap KL, Klaassen B, Vollmer J (1999) Motion control of a snakelike robot. In: Proceedings of 1999 Third European Workshop on Advanced Mobile Robots (Eurobot'99), Zurich, Switzerland, pp 1–8
35. Aoki T, Ohno H, Hirose S (2002) Study on pneumatic mobile robot design of SSR-II using Bridle Bellows mechanism. In: Proceedings of the 41st SICE Annual Conference. SICE 2002, vol. 3, Osaka, Japan, pp 1492–1496. <https://doi.org/10.1109/SICE.2002.1196527>
36. Zhao Z, Ahn CK, Li H-X (2020) Dead zone compensation and adaptive vibration control of uncertain spatial flexible riser systems. *IEEE/ASME Trans Mechatron* 25:1398–1408. <https://doi.org/10.1109/TMECH.2020.2975567>
37. Zhao Z, He X, Ahn CK (2021) Boundary disturbance observer-based control of a vibrating single-link flexible manipulator. *IEEE Trans Syst Man Cybern Syst* 51:2382–2390. <https://doi.org/10.1109/TSMC.2019.2912900>

Publisher's Note Springer Nature remains neutral with regard to jurisdictional claims in published maps and institutional affiliations.